A CNN model with feature integration for MI EEG subject classification in BMI

Arunabha M. Roy[1*]

[1*] *University of Michigan, Aerospace Engineering, Ann Arbor, MI 48109, U.S.A.*

Abstract

Objective. Electroencephalogram (EEG) based motor imagery (MI) classification is an important aspect in brain-machine interfaces (BMIs) which bridges between neural system and computer devices decoding brain signals into recognizable machine commands. However, the MI classification task is challenging due to inherent complex properties, inter-subject variability, and low signal-to-noise ratio (SNR) of EEG signals. To overcome the above-mentioned issues, the current work proposes an efficient multi-scale convolutional neural network (MS-CNN). *Approach.* In the framework, discriminant user-specific features have been extracted and integrated to improve the accuracy and performance of the CNN classifier. Additionally, different data augmentation methods have been implemented to further improve the accuracy and robustness of the model. *Main results.* The model achieves an average classification accuracy of 93.74% and Cohen's kappa-coefficient of 0.92 on the BCI competition IV2b dataset outperforming several baseline and current state-of-the-art EEG-based MI classification models. *Significance.* The proposed algorithm effectively addresses the shortcoming of existing CNN-based EEG-MI classification models and significantly improves the classification accuracy.

1. Introduction :

Brain–computer interfaces (BCI) or brain-machine interface (BMI) enable a direct communication between the brain and external devices [1, 2, 3] which allows rehabilitation of neuromotor disorders [4], robotic control [5, 6, 7], speech communication [8, 9] etc. In general, BMIs can be invasive, non-invasive or synthetic telepathy [2]. Non-invasive method includes

electroencephalography (EEG), functional magnetic resonance imaging (fMRI), magnetoencephalography (MEG), and near-infrared spectroscopy (NIRS) [2, 3]. However, non-invasive BMI through EEG signal collecting through electrodes placed on the scalp has been a popular choice due to its fine temporal resolution, low cost, and user-friendly communication with other electronic devices. Compared with other types of brain signals, EEG has some distinct characteristics such as uniqueness, non-linearity, and non-stationary behaviors which vary with the human brain and the mental state of the particular subjects [10]. Additionally, due to the presence of noise from different muscle artifacts, it poses a challenge to effectively improve the signal-to-noise ratio (SNR) to enhance accuracy in subject classification. Thus, the feature extraction and classification of EEG signals is an important aspect of designing a robust BMI system. The commonly used EEG signals include motor imagery (MI) related mu/beta rhythm (de)synchronization, event-related P300 potentials, and steady-state visually evoked potentials (SSVEPs) [11, 12]. Among these, MI is the most popular in various EEG-based BCI applications [2, 3]. The general workflow of a typical EEG-based MI BCI system is shown in Fig.1 which generally consist of four phases including brain signal acquisition, feature extraction, feature classification, and device control interface. For feature extraction in time-frequency spectrum, wavelet [13] or short-time Fourier-transformation (STFT) [14] have been utilized. Due to the limitation of feature extraction in the same frequency band, the classification accuracy may fall for different subjects. To overcome this, wavelet packet decomposition (WPD) and dynamic frequency feature selection (DFFS) [15] have been employed to obtain better time-frequency features for each subject [16]. However, the procedure is time-consuming and can not be generalized. In regard to feature extraction of EEG signal in space domain, common spatial pattern (CSP) [17], filter bank CSP [18] have shown to be effective in improving accuracy, however, the performance depends on a specific frequency band and does not consider full time-domain feature extraction from different subjects.

With the advancement of deep learning (DL) in recent years, it illustrates superior performance in MI-BCI classification compared to traditional ML methodologies [14] due to the capability of adapting non-linear and non-stationary signals and extracting important feature information [19] from EEG signal automatically. In this regard, there are several studies have been geared towards the EEG signal classification employing DL, in particular, convolutional

neural network (CNN) [14, 20, 21, 22, 23, 24, 25]. A DL model with the combination of CNN and stacked autoencoders (SAE) have been developed which demonstrated the improvement of recognition accuracy for EEG signal classification [14]. In [23], an end-to-end CNN has been designed for efficient MI-EEG signal classification. Some traditional feature extraction methodologies such as wavelet transform (WT) from time-frequency images have been incorporated in CNN for subject classification [26]. A DNN Scheme based on restricted Boltzmann machines (RBM) for MI classification has been proposed in [27]. In addition, EEGNet framework [28] based on compact CNN has been proposed for MI and P300 visual-evoked potentials which demonstrated improvement of classification accuracy compared to the state-of-the-art methods. Along similar line, a deep transfer CNN framework based on the VGG-16 CNN model pre-trained on the ImageNet and a target CNN model for MI EEG signal classification has been proposed in [29]. Furthermore, a 1-D multi-scale CNN [30] based on conditional empirical mode decomposition (CEMD) has been developed which correlates the original EEG signal and intrinsic modal component (IMF) to encode event-related synchronization/de-synchronization (ERS/ERD) information between the channels achieving higher accuracy for EEG signals classification. Additionally, a multiple bandwidth method with optimized CNN framework [31] has been designed for BMI classification with EEG-fNIRS signals. More recently, a hybrid-scale CNN architecture [32] for EEG MI classification has been proposed which demonstrates significant improvement in classification accuracy.

Although, the CNN-based models have achieved better results, there are several issues which cause to hinder the accuracy and performance of the classifier for EEG MI classification. Firstly, most of the CNN-based models consider only a single convolution scale which is not sufficient to extract distinguishable features of several non-overlapping canonical frequency bands of EEG signal efficiently. Secondly, intrinsic feature extraction of the input signal is often ignored which limits CNN's ability to learn more semantic features from the raw EEG data. Moreover, feature extraction has not been designed to fully integrate into the DL workflow which is the main bottleneck for the deployment of real-time BCI applications with high classification accuracy. Thirdly, one of the common issues of CNN-based models is the lack of sufficient training data which restrain to achieve high classification accuracy for EEG-based MI-BCI classifier.

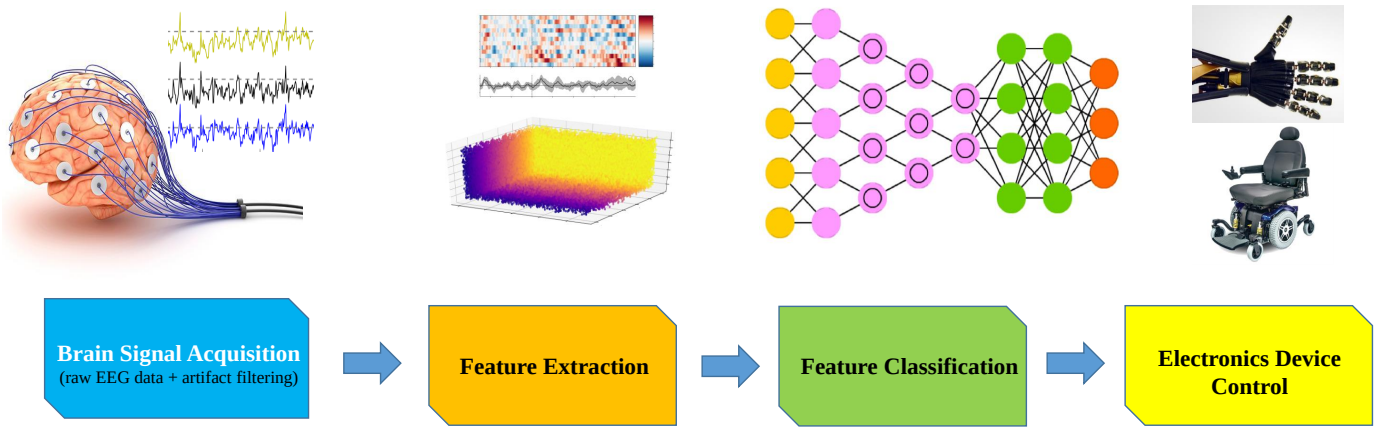

Figure 1: The general workflow of a typical EEG-based MI-BCI system consist of brain signal acquisition, feature extraction, feature classification, and device control interface.

In order to address the aforementioned challenges and shortcomings, an efficient multi-scale convolutional neural network (MS-CNN) has been proposed for EEG-based MI classification. In the model, a multi-scale convolution block (MSCB) with different convolutional kernel sizes has been designed to extract the effective features of EEG signals from multiple scales for four different frequency bands δ, θ, α, and β from original EEG data for MI classification. Moreover, important intrinsic and user-specific features including differential entropy (DE) and neural power spectra (NPS) characteristics have been extracted from the original EEG data and integrated into the proposed algorithm to improve the accuracy and performance of the model. Additionally, different data augmentation (DA) methods such as Gaussian noise (GN), signal segmentation and recombination (S & R), window slicing (WS), and window wrapping (WW) have been employed to further improve the accuracy and robustness of the proposed classifier by increasing training EEG data. It has been found that the current algorithm significantly outperforms several baselines and the current state-of-the-art EEG-based MI classification models with an average classification accuracy of 93.74% on BCI Competition IV2b dataset. Current study provides an effective and efficient framework for designing high performance real-time MI-BCI system.

2. Dataset and description of experimental method :

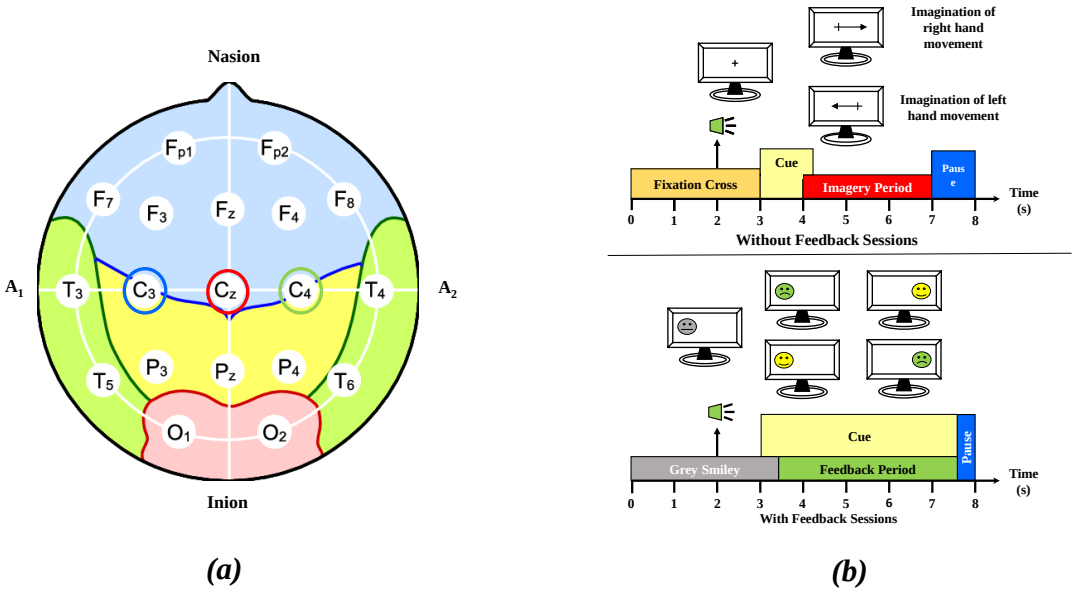

Figure 2: (a) Schematics of electrodes positioning of C_3, C_Z, and C_4 in standardized international 10-20 electrode system ; (b) timing scheme of each trial including first two sessions (top) and remaining three sessions (bottom).

In the present work, BCI competition IV 2b dataset [33] has been utilized to evaluate the efficiency and accuracy of the proposed MS-CNN model. The 2b datasets contain EEG data collected from nine healthy subjects. For each subject, the EEG signal data has been recorded and collected from three bipolar EEG channel electrodes with a sampling frequency of 250 Hz. These electrodes (i.e., C_3, C_Z, and C_4) have been positioned according to standardized international 10-20 electrode system [34] as shown in Fig. 2-(a). In order to eliminate the power line signal noise, a band-pass filter allowing EEG signal frequency between 0.5 Hz and 100 Hz with a notch filter at 50Hz was implemented. Additionally, the electrooculogram (EOG) has been recorded using three monopolar electrodes [35, 36]. In the dateset, two types of MI classification tasks has been performed by each subject which include left (class 1) and right-hand movement (class 2) imagination. From the given dataset, there is a total of 5 sessions were considered for each of the subjects. For each subject case, the first two sessions consisting of 120 trials were collected without feedback in EEG signal data. Whereas, the remaining three sessions of 160 trials were recorded with EEG feedback. The schematic of each trial and corresponding timing stamp has been depicted in Fig. 2-(b). For example, consider the first two sessions, the successive events are as following order: at the start of each

trial (i.e., t=0) a fixation cross appears; followed by a cue in the form of an arrow at t=3 s to t=4.25 s indicating two distinct MI tasks at once; finally, the subject performs left and right-hand movement imagination according to arrow direction from t=4 s to t=7 s [35, 36, 37].

3. Proposed CNN model:

In recent years, CNN has demonstrated significant performance improvement outperforming traditional ML approaches [38] in various applications such as object detection and computer vision [39, 40]. The MI subject classification from the raw EEG signal with high variability and non-stationary noise is a challenging task. In this regard, CNN can be an effective method for extracting the most relevant features and learning the hierarchical representations of high dimensional EEG time series data. CNN is a feed-forward network that is usually comprised of the following components: input layer, convolution (Conv) layer, pooling (Pool) layer, fully connected (FC) layer, and output layer. Generally, the CNN network consists of alternating convolution and pooling layers for extracting features, and a fully connected layer at the end for final classification. Mathematically, the convolution process can be expressed as :

$$S_j^d = f\left(\sum_{i \in M_j} S_i^{d-1} * w_{ij}^d + b_i^d\right) \tag{1}$$

Where S_j^d is the j^{th} feature information in the d^{th} Conv ; S_i^{d-1} and b_i^d are the i^{th} feature map and bias term corresponding to $d-1^{th}$ and d^{th} Conv, respectively; w_{ij}^d represents connecting weight between i^{th} feature of the $d-1^{th}$ layer and j^{th} feature of the d^{th} layer; $*$ denotes convolution operator; M_j represents input feature collection; $f(\bullet)$ represents the activation function which can be hyperbolic tangent $f(x) = tanh(x)$, sigmoid type $f(x) = 1/(1+e^{-x})$, or rectified linear units (ReLU) $f(x) = max(0, x)$ etc. The main functionality of pooling layer is to reduce the spatial size of the representation and the number of network parameters while preserving important and relevant features information. The fully connected layer at the end of the CNN transforms the high dimensional feature map obtained from the previous layer into 1D array. Finally, it is connected to the Softmax layer to predict the classification result. However, in EEG signals, there are several non-overlapping canonical frequency bands corresponds to various distinct behavioral state[41, 42]. Each frequency pattern represents a qualitative

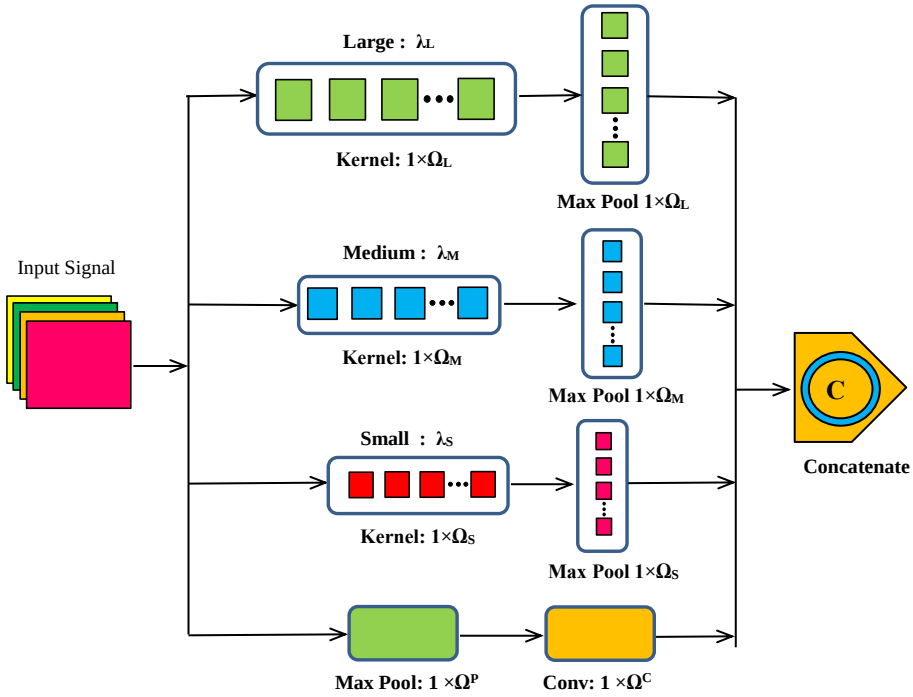

Figure 3: Generalized schematic of network structure for proposed multiscale convolution block (MSCB) consisting of three different convolution scale: large (λ_L), medium (λ_M), and small (λ_S) for multi-scale feature extraction.

assessment of awareness during MI tasks. The low frequency δ- bands (1-4 HZ) was found to carry significant class-related information [2, 43, 44]. Additionally, in movement-related MI-BCI systems, α (8-13 HZ)and β (13-30) rhythms are important due to their high temporal resolution [45]. An increase and decrease of power spectrum in the β and α- bands results in event-related synchronization (ERS) and event-related desynchronization (ERD), respectively [46, 47]. Recently, it has been revealed that θ-band (4-8 Hz) significantly differs between the left/right-hand MI tasks which plays an important role in MI-BCI classification process [32, 48, 49]. Thus, in the current study, we have considered four non-overlapping frequency bands including δ, θ, α, and β for feature extraction from original EEG data in our proposed CNN model. A filter bank of 1-4 Hz, 4-8 Hz, 8-13 Hz, and 13-30 Hz has been employed to extract EEG signal information in corresponding frequency bands.

3.1 multi-scale convolution block (MSCB): In the proposed MSCB network, convolution block λ_L has a relatively large convolution kernel size $1 \times \Omega_L$ which can capture the overall feature map of the EEG signal. Relatively medium convolution kernel size $1 \times \Omega_M$ in

Table 1: Main network parameters of generalized multi-scale convolution block (MSCB) as shown in Fig. 3.

Layer type	Kernel size	No of Kernel	Stride	Padding	Feature map
Convolution λ_L	$\Omega_L^C = 5$	$N_K^{\lambda_L} = 14$	$S_K^{\lambda_L} = 1$	SAME	$L_s \times N_K^{\lambda_L}$
Max Pool λ_L	Ω_L^P	–	$S_P^{\lambda_L}$	SAME	$(L_s/S_P^{\lambda_L}) \times N_K^{\lambda_L}$
Convolution λ_M	$\Omega_M^C = 3$	$N_K^{\lambda_M} = 14$	$S_K^{\lambda_M} = 1$	SAME	$L_s \times N_K^{\lambda_M}$
Max Pool λ_M	Ω_M^P	–	$S_P^{\lambda_M}$	SAME	$(L_s/S_P^{\lambda_M}) \times N_K^{\lambda_M}$
Convolution λ_S	$\Omega_S^C = 1$	$N_K^{\lambda_S} = 14$	$S_K^{\lambda_S} = 1$	SAME	$L_s \times N_K^{\lambda_S}$
Max Pool λ_S	Ω_S^P	–	$S_P^{\lambda_S}$	SAME	$(L_s/S_P^{\lambda_S}) \times N_K^{\lambda_S}$
Max Pool λ	Ω^P	-	S_P^{λ}	SAME	$(L_s/S_P^{\lambda}) \times N_f$
Convolution λ	Ω^C	$N_K^{\lambda} = 24$	$S_K^{\lambda} = 1$	SAME	$(L_s/S_P^{\lambda}) \times N_K^{\lambda}$
Concatenate	-	14 ? -	-	-	$(L_s/S_P) \times 56$

Table 2: Main network parameters of proposed multiscale CNN (MS-CNN) model as shown in Fig. 4.

Layer type	Kernel size	No of Kernel	Stride	Padding	Feature map
MSCB	-	-	-	-	$(L_s/S_P) \times 56$
CL	Ω^{CL}	112	$S_{CL} = 1$	SAME	$(L_s/S_P) \times 112$
MP	Ω^{MP}	-	S_{PL}	SAME	$L_s/(S_P \times S_{PL}) \times 112$
1^{st} FC	-	-	-	-	400
Dropout layer	-	-	-	-	-
2^{nd} FC	-	-	-	-	300
Output layer	-	-	-	-	2

convolution block λ_M can preserve relatively coarse grain feature information. Finally, convolution block λ_M with small kernel size $1 \times \Omega_S$ can efficiently collect fine-grain localize information.

3.2 Multi-scale CNN (MS-CNN): The proposed multi-scale CNN architecture has been presented in Fig. 4. At first, the inputted EEG signal has been divided into four different frequency bands channels and passed through corresponding MSCB blocks (i.e., MSCB_i, $i = \delta, \theta, \alpha$, and β) to obtain multi-scale features from the EEG signal as shown in Fig. 4. These MSCB blocks have been connected to convolution and then max-pooling layers. The kernel size of $1 \times \Omega^{CL}$ in convolution layer with stride $S_{CL} = 1$ can preserve relatively coarse fine-grain feature information. The subsequent max-pooling layer reduces the size of feature information utilizing filter size of Ω^{MP} with stride $S_{PL} = 5$. The extracted features from the max-pooling layer have been passed through the first flatten layer for feature fusion. During feature fusion, 2D feature vectors are transformed to 1D feature by row concatenation process for all four brunches as shown in Fig. 4. Finally, further concatenation operation transforms all the 1D features from the four branches into a 1D array which has been used as the input to the fully connected layer with number of hidden units N_h. The output of the network is obtained by utilizing the Softmax layer that performs multi-class classification of EEG signals. The proposed network utilizes ReLU as the primary activation function which accelerates the

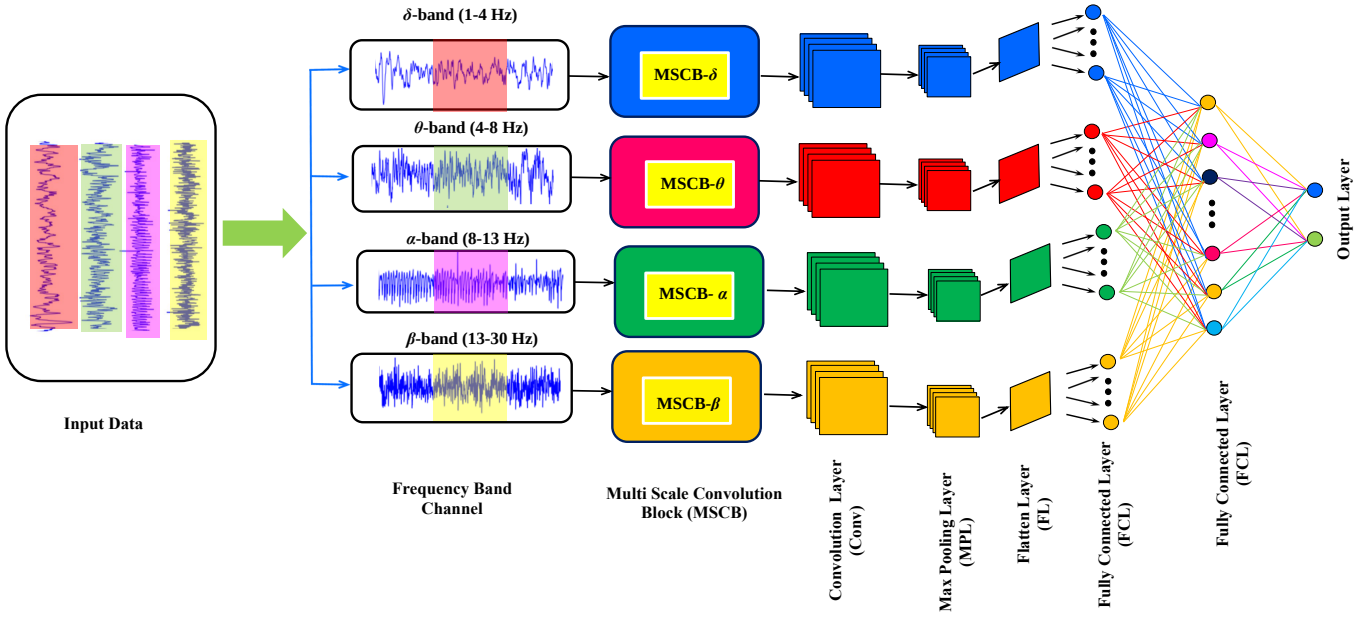

Figure 4: The schematic of proposed multi-scale CNN (MS-CNN) network architecture consisting of four different MSCB as shown in Fig. 3 for efficient multi-scale feature extraction for different non-overlapping frequency bands.

optimization process of the MS-CNN network and increases the classification accuracy for MI-BCI application [30]. Moreover, cross-entropy has been used as a loss function to optimize the model during training. The cross-entropy L_{CE} for n classes can be defined as:

$$L_{CE} = -\sum_{i=1}^{n} t_i log(p_i) \tag{2}$$

Where t_i is the truth label; p_i is the Softmax probability for i^{th} class. In the proposed model, the trial matrix size of $1 \times N_{L_s}$ (where N_{L_s} is the numeber of data points of each EEG trials) from EEG signal data has been inputted in the MS-CNN; where L_s is the segment of EEG signal in interest and N_c is the number of EEG channels. The time period of a MI trial ranges from 3.5s to 7.5s as shown in Fig. 2-(b). Thus, with the sampling frequency of 250 Hz, we obtain a trial of $L_s = 4s$ with N_{L_s}=1000 data points.

4. EEG Feature Extraction:

Due to inter-subject variability of the EEG signals, the accuracy of the classifier often diminish. Thus, it is critical to extract the user-specific features information from EEG data to improve classification accuracy in MI based BCIs. Although there are many features such as statistical, time-domain, frequency-domain, wavelet, auto-regressive coefficients can be extracted from EEG signals [52], however, in the proposed framework, two highly discriminant user-specific features have been extracted and integrated in the MS-CNN model which improve the accuracy and performance of the model.

4.1 Differential entropy: From the MI-EEG signal data segment, differential entropy (DE) feature has been extracted which demonstrated superior performance compared to commonly used features [53]. The DE of a given EEG signal X satisfying the Gauss distribution $N(\mu, \sigma^2)$ can be expressed as

$$h(X) = -\int_{-\infty}^{\infty} \frac{1}{\sqrt{2\pi\sigma^2}} e^{-\frac{(x-\mu)^2}{2\sigma^2}} \log\left(\frac{1}{\sqrt{2\pi\sigma^2}} e^{-\frac{(x-\mu)^2}{2\sigma^2}}\right) dx = \frac{1}{2}\log 2\pi e\sigma^2 \tag{3}$$

Where σ is the standard deviation, ζ is the mean value. For a particular EEG signal segment, DE feature is equivalent to the logarithm energy spectrum in a distinct frequency band. Thus, a bandpass filter has been employed to extract four different frequency bands δ (1–4 Hz), θ

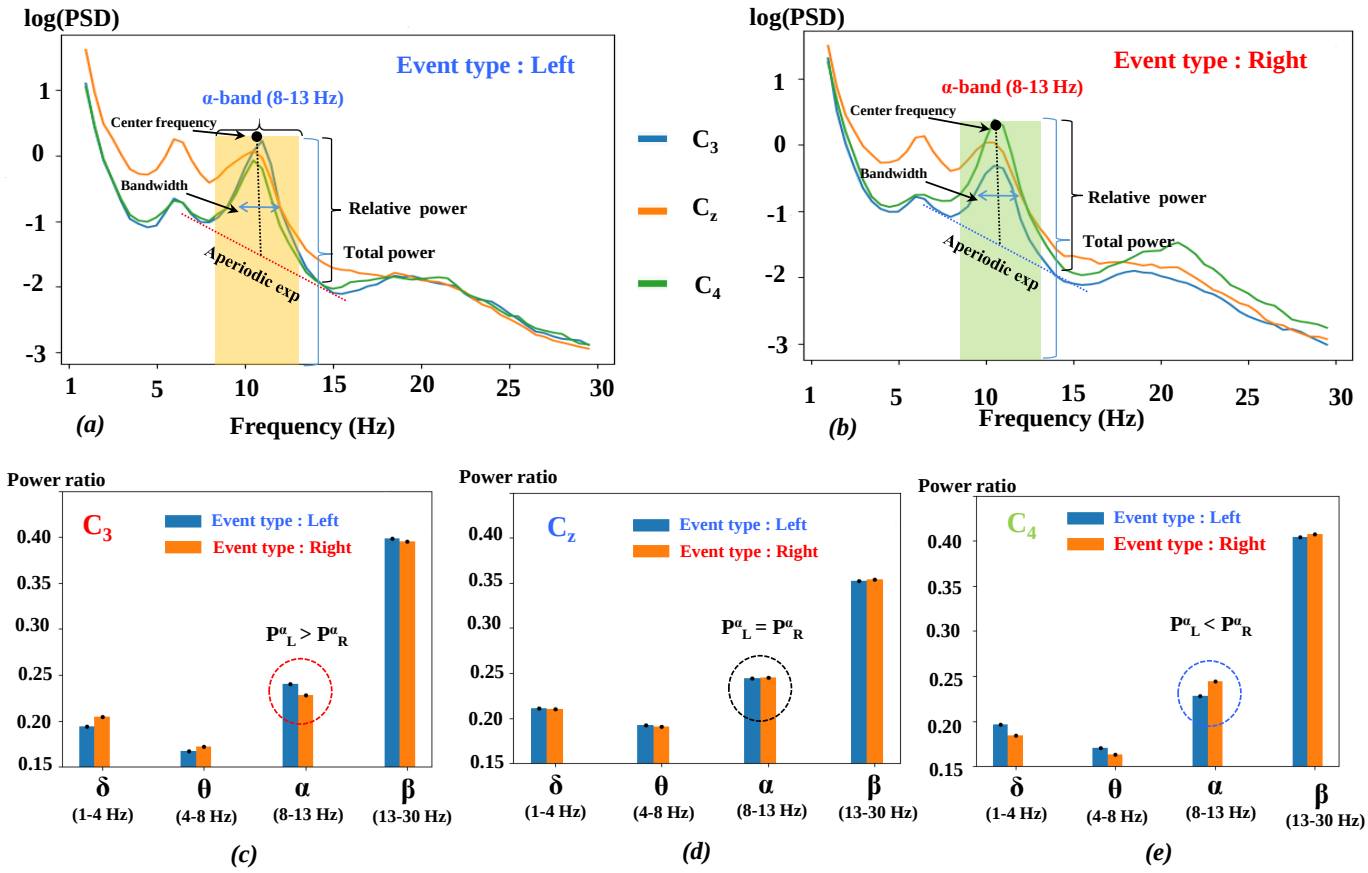

Figure 5: (a, b) NPS containing strong peak in α band (8-13 Hz, yellow and green region) and secondary θ (not marked) with overlapping nature of periodic and aperiodic spectral features for left and right event type, respectively ; (c, d, e) comparison of power ratio in left and right event type for four different canonical frequency range from the electrodes C_3, C_Z, and C_4.

(4–8 Hz), α (8–13 Hz), and β (13-30 Hz) from each EEG channel. Subsequently, short-time Fourier transform has been employed with a non-overlapped hamming window of 4 s on trial EEG signal segment consist of 1000 data points to obtain the energy spectrum of each specified frequency band. Finally, the DE feature has been extracted by calculating the logarithm energy spectrum for each of the aforementioned four frequency bands from single channel. After feature extraction, the shape of the DE feature matrix for each selected EEG segments has been concatenated with MS-CNN main feature matrix.

4.2 Neural power spectra: Typically, EEG signal data has been analyzed using only canonically defined frequency bands, ignoring the aperiodic component which may compromise physiological interpretations. However, the EEG neural data contains both periodic and

aperiodic components [42]. Recently, the neural power spectra (NPS) model has been introduced which combines both aperiodic component and putative periodic oscillatory peaks [42]. In this model, the neural PSD has been characterized by the power, specific center frequency, and bandwidth without requiring predefining specific EEG frequency bands and controlling for the aperiodic component. Additionally, the characteristics of these aperiodic components allow one to measure and compare the $1/f$-like components between inter-subject variability of the EEG signals. This model has been utilized to extract periodic and aperiodic features of EEG data in the present study. To measure the periodic activity, the power relative to the aperiodic component has been calculated with each peak can be described by Gaussian in terms of parameters a, c and w, where a is the height of the peak, over and above the aperiodic component; c is the center frequency of the peak; w is the width of the peak; F is the array of frequency values. Each Gaussian, n referred to as $G(F)_n$ can be expressed as [42]:

$$G(F)_n = a\, e^{-\frac{(F-c)^2}{2w^2}} \tag{4}$$

Whereas, the aperiodic activity component without any characteristic frequency can be expressed as the function $L(F)$ as follows:

$$L(F) = b - \log(k + F\chi) \tag{5}$$

Where b is the broadband offset; χ is the exponent of the aperiodic fit; k is the 'knee'. Finally, across a set of frequencies F, NPS can be expressed as $NPS(F) = G(F)_n + L(F)$. For better clarity, an example of NPS containing a strong peak in α band with overlapping nature of periodic and aperiodic spectral features for two classes have been shown in Fig. 5-(a, b). Consequently, the power ratio (spectral power in the bin normalized by power in all spectral bins) for four different canonical frequency range from the electrodes C_3, C_Z, and C_4 reveals that the α range power decreases as shown in Fig. 5-(c, d, e) on the opposite (i.e. contralateral) hemisphere when MI on one side is performed for a particular class. The apparent differences between the different electrode's PSDs, in particular, relative PSDs of C_3 (see Fig. 5-c) and C_4 (see Fig. 5-e) channels vary between the two MI classes. Clearly, NPS is a highly discriminant user-specific feature that improves the accuracy and performance of the model significantly (see section 6.3). In the present study, NPS features containing periodic (c, w, and P_{band}) and aperiodic parameters (b, k, and χ) have been extracted for each of the four frequency bands for

each channel and finally concatenated with MS-CNN main feature matrix as shown in Fig. 8.

5. Data augmentation of EEG signal:

In DL based MI-BCI system, the accuracy of the MI classifier is greatly dependent on the volume of EEG training data. Without sufficient data, the accuracy may drop. Hence, to improve the accuracy and robustness of the CNN classifier, data augmentation (DA) methods can be employed to generate new sample data from existing EEG training sample [54]. However, improper DA might lead to a decrease in the performance of the classifier. In the present study, four different types of DA methods have been chosen and implemented specifically for EEG-based MI-BCI systems to increase the volume of EEG data during training and improve the performance of the classier (see section 6.4).

5.1 Gaussian noise: In the first DA method, noise has been added to the original training data. The EEG signal has strong randomness and highly non-stationary characteristics. Thus, randomly added local noise may alter the important EEG feature. In order to preserve the important local feature of EEG data, Gaussian noise (GN) has been added to the original training data [53]. The probability density function P_G of a Gaussian random variable ξ can be expressed as follows:

$$P_G(\xi) = \frac{1}{\sigma\sqrt{2\pi}} e^{-\frac{(\xi-\zeta)^2}{2\sigma^2}} \tag{6}$$

Where σ is the standard deviation, ζ is the mean value. In the present work, $\zeta = 0$ has been prescribed to ensure that the amplitude of the original EEG signal remain unchanged after the addition of noise. During DA, different noise intensity i.e., σ=0.001, 0.005, 0.01, 0.05, 0.10, 0.25, and 0.5 have been considered.

5.2 Signal segmentation and recombination in time domain: Additionally, EEG data transformation including signal segmentation and recombination (S & R) has been utilized as a second DA method to further expand the dataset. In this procedure, each training EEG trial for the particular class has been subdivided into multiple segments and then new trials are generated by combining segments collected from different and randomly selected trials

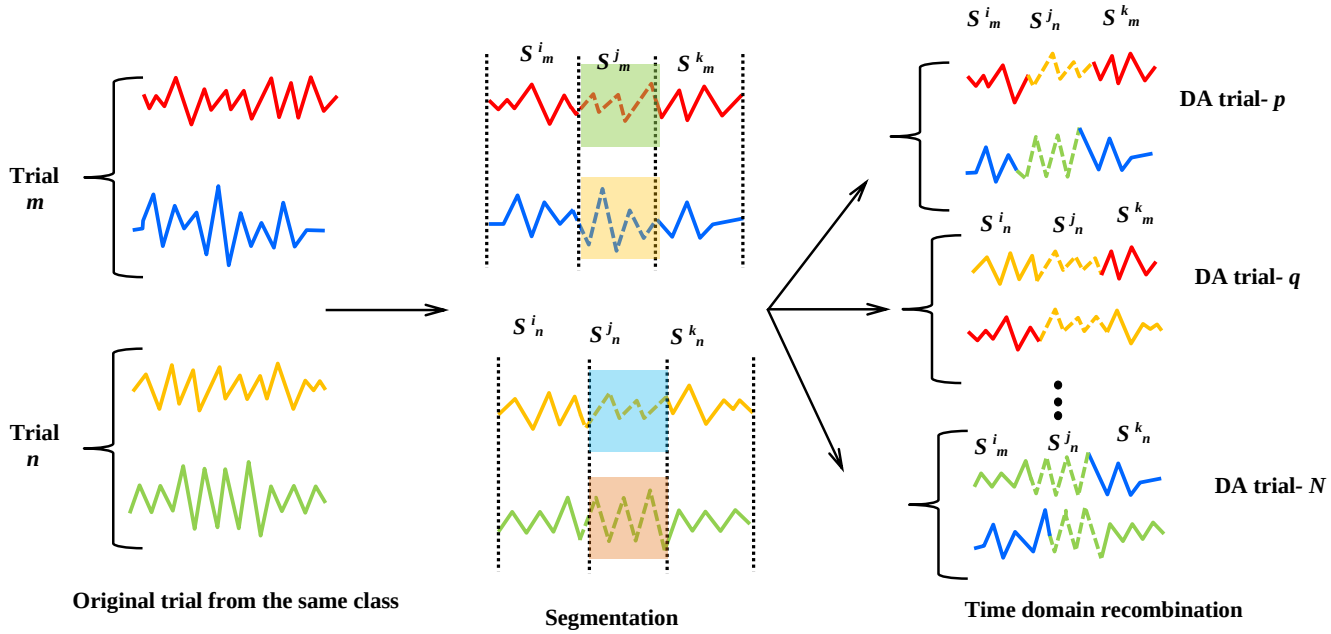

Figure 6: Procedure of EEG signal segmentation and recombination in time domain for data augmentation.

from the same training class data [55]. If $\Delta = \{S^i\}, i \in [1, n]$ is the set of total n number of EEG training data for given class, each training EEG trial S^i for the particular class has been subdivided into K consecutive and non-overlapping segments S^i_K and then generating a new trials $\tilde{S}^j = [S^j_m, S^j_n, \ldots S^j_n]$ by combining segments from different and randomly selected training trials from the same class. The schematic of S & R - DA procedure has been shown in Fig. 6. Considering the original trials S_m and S_n from the same class have been segmented into $[\ldots, S^i_m, S^j_m, S^k_m, \ldots]$ and $[\ldots, S^i_n, S^j_n, S^k_n, \ldots]$. These segments have been recombined in time domain to obtain N additional DA trials. In the present work, input EEG trials (i.e. left/right-hand MI) have been considered as same label with each trial has been segmented into 4 division with 250 data points (i.e., 1 sec long segment).

5.3 Window slicing: In the window slicing (WS) DA method, EEG time series data have been extracted in slices and classification has been performed at different slice levels [56]. During training, each slice of the corresponding class has been assigned to the same class where the size of the slice is one of the parameters for the DA. In the present work, a window of 90% of the training EEG data has been chosen randomly and interpolated back to the original size

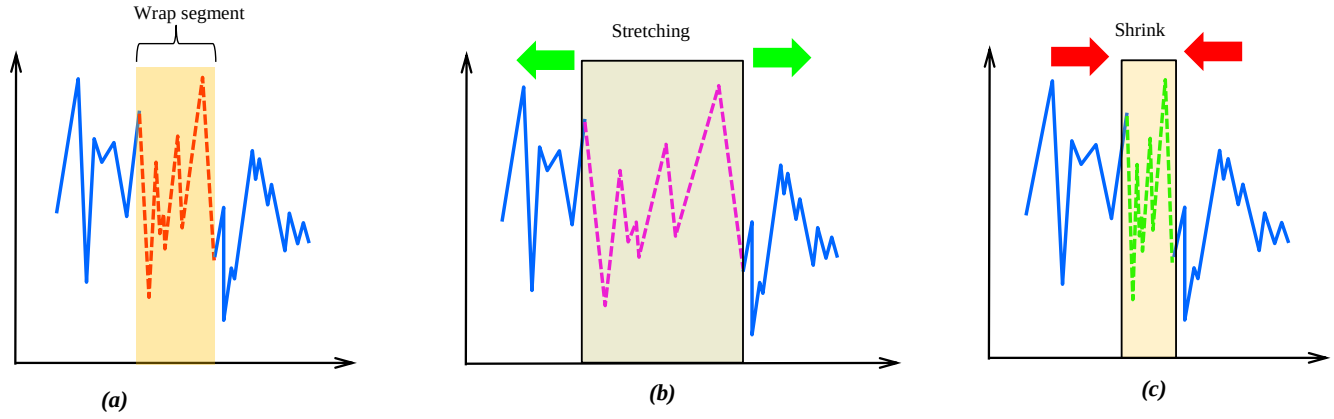

Figure 7: Schematic of window warping data augmentation technique for EEG signal.

to fit with the classifier [56, 57].

5.4 Window Warping: In the last DA technique, window warping (WW) [56] DA has been utilized which expands or contracts random windows of the EEG training data by some specific value. Considering the length of the original EEG signal as a parameter, WW warps a randomly selected segment as shown in Fig. 7. Although, WW generates input time series of different lengths, however, the issues can be overcome by performing DA on transformed EEG data having equal lengths [56]. The present study considers a random window of 10% of the original EEG data and wrapped it by speeding it up by 2 or slowing it down by 0.5.

6. Results and discussion:

In this section, the performance and accuracy of the proposed model have been discussed and compared with several existing methods. The BCI competition IV-2b EEG dataset includes 9-subject and 2-class motor-imagery (right hand, left hand) with five sessions for each subject. The first two sessions (identifiers: 01T and 02T) have been used to train the classifier for all models [35]. The third session (identifiers: 03T) has been employed during validation. The last two sessions (identifiers: 04E and 05E) have been strictly utilized for evaluating the corresponding trained classifier [35, 36]. The EEG trial length of $L_s = 4s$ with N_{L_s}=1000 data points has been used. The proposed MS-CNN model has been fine-tuned on the valida-

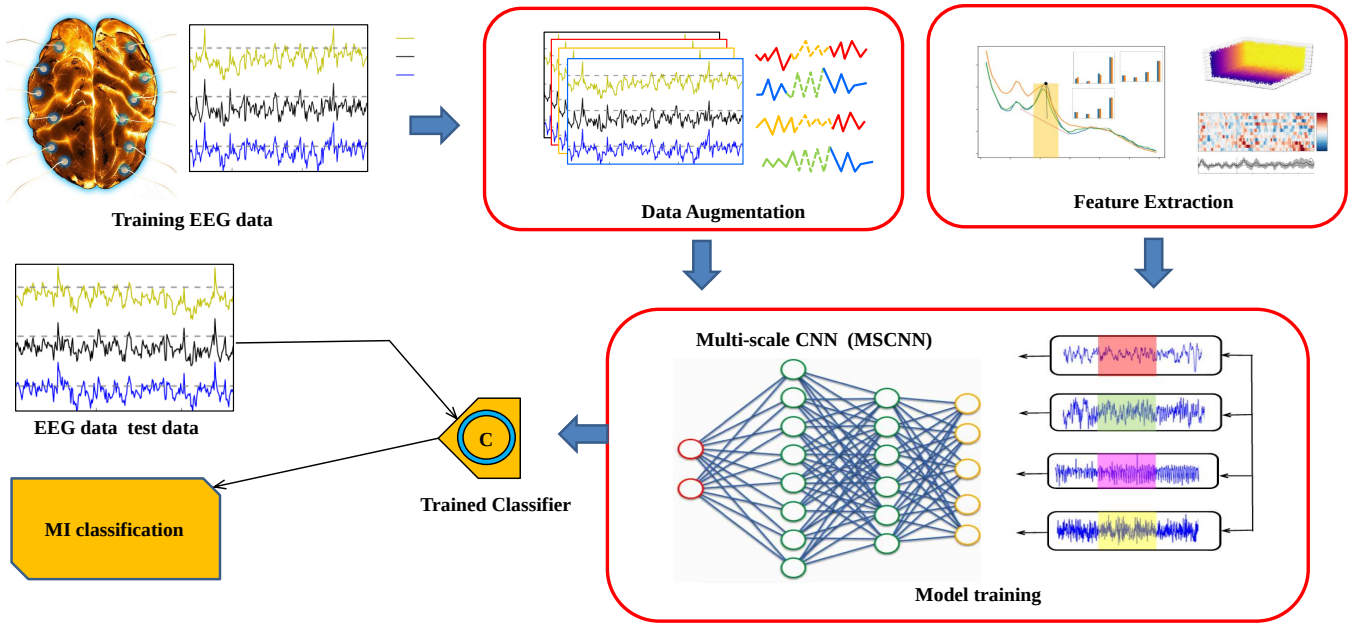

Figure 8: Flowchart representing the overall workflow of the proposed framework for EEG-based MI BCI system based on DA and feature integration.

tion set and then applied to testing sets. The final fine-tuned network parameters $\Omega_S = 1$, $\Omega_L^P = \Omega_M^P = \Omega_S^P = \Omega^P = 5$, $\Omega_M = 3$, $S_P^{\lambda_L} = S_P^{\lambda_M} = S_P^{\lambda_S} = S_K^{\lambda} = 5$ and $\Omega_L = 5$ have been prescribed. During training, a batch size of 16 has been chosen to optimize the convergence speed and achieve higher classification accuracy. In the proposed model, stochastic gradient descent (SGD) has been utilized as a training strategy with 500 epochs prescribing an exponential decay rate of 0.8 for optimizing the cross-entropy loss function. Due to the high conditionality of the optimization procedure in MI-BCI classification, SGD reduces the computational burden by achieving faster convergence. The initial learning rate is set to 0.001 and the learning rate decays every 30 epochs with an exponential decay rate of 0.5. Lastly, L2 regularization with a regularization parameter value of 0.02 and dropout technique with a dropout probability value of 0.5 (in the first FC layer) have been prescribed to prevent over-fitting. Finally, the models were implemented using the Keras API with TensorFlow as the lower level backend library. Additionally, MNE v0.23 [58], PyEEG [59], NeuroDSP [60], and FOOOF [61] libraries have been utilized for data pre-processing, feature extraction, spectral-domain and NPS analysis. The flowchart representing the overall workflow of the proposed framework has been shown in Fig. 8. For each subject, the experiment has been executed 10 times. The accuracy per-

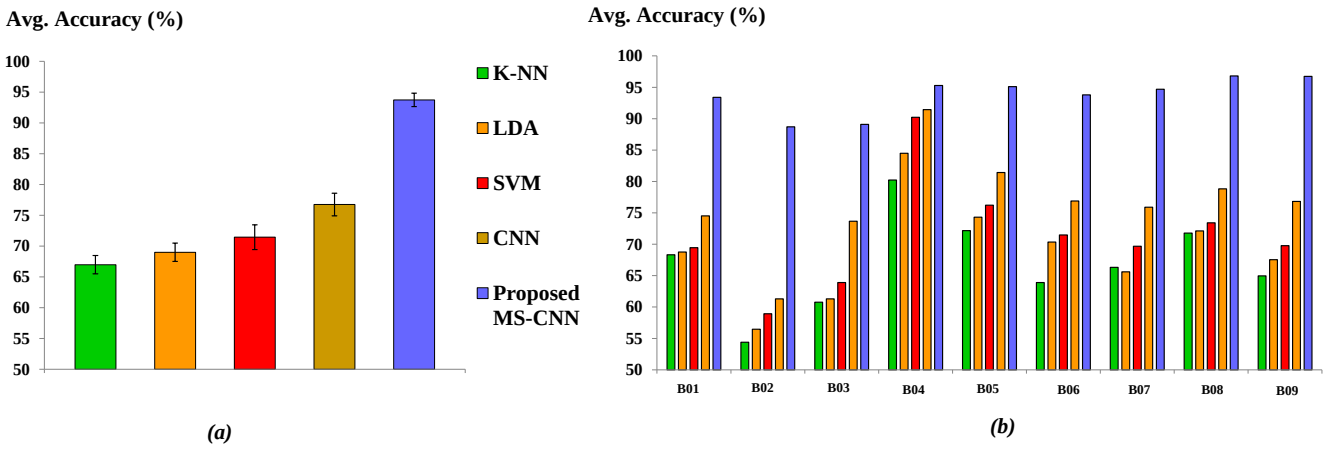

Figure 9: Comparison bar chart of (a) average accuracy with SE (in %) (b) average accuracy of each subject between K-NN, LDA, SVM, CNN, and proposed MS-CNN models.

formance of the proposed framework is evaluated on the prepared testing set. The average classification accuracy and standard error (SE)= $s/\sqrt{n}$ (s is the sample standard deviation; n is the sample size) have been calculated from the test datasets.

6.1 Performance comparison with different algorithms: In this paper, the average classification accuracy has been used to evaluate different classification models. The global averaged accuracy is defined as the ratio of the number of correctly classified samples to the total number of samples. The performances of the proposed MS-CNN model has been compared with three popular traditional ML models in MI-BCI classification: K-nearest neighbor(K-NN), linear discriminant analysis (LDA), and support-vector machine (SVM) as the baseline models. Additionally, the standard CNN model has also been considered as the baseline DL model. Note, the standard CNN structure consisting of 4 convolution and max-pooling layers is deeper than the MS-CNN model. For fair comparison, all feature extraction and data augmentation methods have been applied in all aforementioned baseline models. Additionally, model hyper-parameters have prescribed the same as the proposed model. As shown in Table 3, the proposed MS-CNN has obtained the best accuracy across all subjects among all baseline models with an average accuracy of 93.74% for the BCI competition IV-2b dataset. Compared to K-NN, LDA, and SVM, it has achieved d 26.76%, 24.75%, and 26.96% improvement in average classification accuracy, respectively. The proposed model has achieved 16.92% accuracy

Table 3: Average accuracy values of each subject from K-NN, LDA, SVM, CNN, and proposed MS-CNN models where bold indicates the best result from the corresponding model

Subject	**Average Accuracy**				
	***K*-NN**	**LDA**	**SVM**	**CNN**	**MS-CNN**
B01	68.32	68.77	69.45	74.52	**93.45**
B02	54.39	56.46	58.92	61.29	**88.71**
B03	60.77	61.29	63.89	73.67	**89.14**
B04	80.22	84.49	90.22	91.45	**95.37**
B05	72.17	74.32	76.23	81.43	**95.11**
B06	63.89	70.35	71.47	76.89	**93.82**
B07	66.32	65.60	69.68	75.89	**94.70**
B08	71.17	72.12	73.41	78.83	**96.81**
B09	64.97	67.55	69.77	76.82	**96.73**
Avg. Accuracy with SE	66.98 $\pm$1.67	68.99 $\pm$1.49	71.45 $\pm$2.01	76.76 $\pm$1.84	**93.74**$\pm$1.09

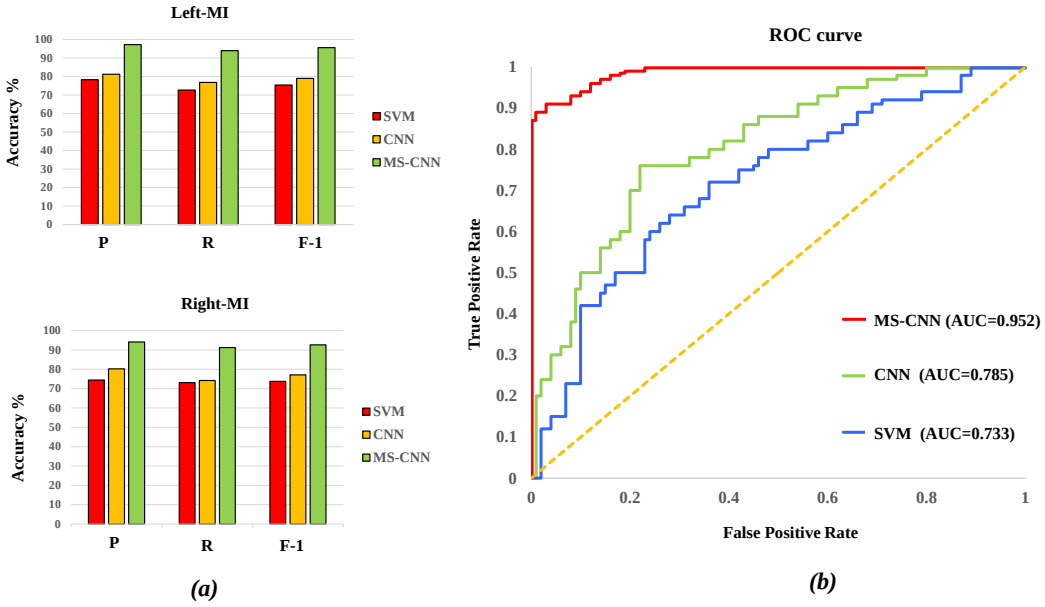

Figure 10: (a) Comparison bar chart of P, R, F-1 (in %) for the two different MI (left and right hand); (b) ROC curves and corresponding AUC values obtained from SVM, CNN, and MS-CNN models.

improvement over the standard CNN model as shown in Fig. 9 indicating the superior performance of MS-CNN. Additionally, the MS-CNN model has the lowest SE value which indicates that the proposed model has the capability of the subject-independent representation of EEG data and better generalization of the classifier compared to other baseline methods. Furthermore, the performance of MS-CNN model on the recognition of two different MI classes (left and right hand) have been measured by precision (P), recall (R), and F1-score and compared with SVM and standard CNN model as shown in Fig. 10- (a). For binary classification, sample data can be classified into four different categories: true positive (TP), false positive (FP), true negative (TN), and false negative (FN), based on the true class and the model-predicted class. The evaluation matrices P, R, F1 can be defined as

$$P = \frac{TP}{(TP + FP)}; \qquad R = \frac{TP}{(TP + FN)} \tag{7}$$

$$F1 = \frac{2PR}{(P + R)}. \tag{8}$$

The larger values of P, R, F1 indicate better performance of the model. The proposed MS-CNN model has achieved best P, R, F1 values of 97.25%, 93.99%, 95.59% and 94.15%, 91.22%,

92.66% for left and right MI, respectively. Finally, ROC (receiver operating characteristic) curve has been plotted from the true positive rate (TPR) or R (in the ordinate) and false positive rate (FPR) data (in the abscissa) from SVM, standard CNN, and MS-CNN result as shown in Fig. 10- (b). The area under the ROC curve is expressed in AUC and ranges from 0.5 to 1. The closer the AUC is to 1.0, the higher the performance of the model. As shown in Fig. 10- (b), SVM, standard CNN, and MS-CNN have achieved AUC values of 0.733, 0.785, and 0.952, respectively indicating the best performance of MS-CNN compared to other classification models. The total number of trainable network parameters of MS-CNN is 297,056 compared to 334,236 of the standard CNN. Both models take a similar average time-frame (within 2 min) to train, whereas standard CNN takes a slightly higher training time due to a higher number of trainable parameters. The comparison demonstrates that the MS-CNN can have significantly better accuracy and learning capability for different subject classes with less training time. It is noteworthy to mention, both DL-based standard CNN and MS-CNN models demonstrate superior performance in MI classification accuracy than traditional baseline ML models for all subjects. The comparison illustrates the advantages of the DL model for its strong feature extraction capability and capturing abstract-advanced information among different subjects compared to traditional ML methods in EEG-based MI-BCI systems.

6.2 Influence of convolution kernel size : In this section, different combinations of the convolution kernel size (i.e, Ω_S, Ω_M, and Ω_L) in MSCB have been studied to explore the influence of kernel sizes on the performance of the model. From the comparison as shown in Fig. 11, it can be shown that with increasing kernel size, in particular, for combinations ($\Omega_S = 3$, $\Omega_M = 7$, $\Omega_L = 9$) and ($\Omega_S = 3$, $\Omega_M = 9$, $\Omega_L = 11$) classification accuracy drops to 89.78% and 87.39%, respectively. However, the combination of relatively small kernel size, classification accuracy, as well as speed, improves. Comparing all the results, it can be found that the best classification result corresponds to ($\Omega_S = 1$, $\Omega_M = 5$, $\Omega_L = 7$) with an accuracy of 93.99%. However, in this study, combinations of $\Omega_S = 1$, $\Omega_M = 3$, and $\Omega_L = 5$ has been selected which is computationally more efficient for real-time MI BCI system compromising only 0.25% accuracy compared to result corresponds to ($\Omega_S = 1$, $\Omega_M = 5$, $\Omega_L = 7$). Additionally, the selected combination of kernel scales has achieved the smallest SE value of 1.09%, which is 0.20% lower

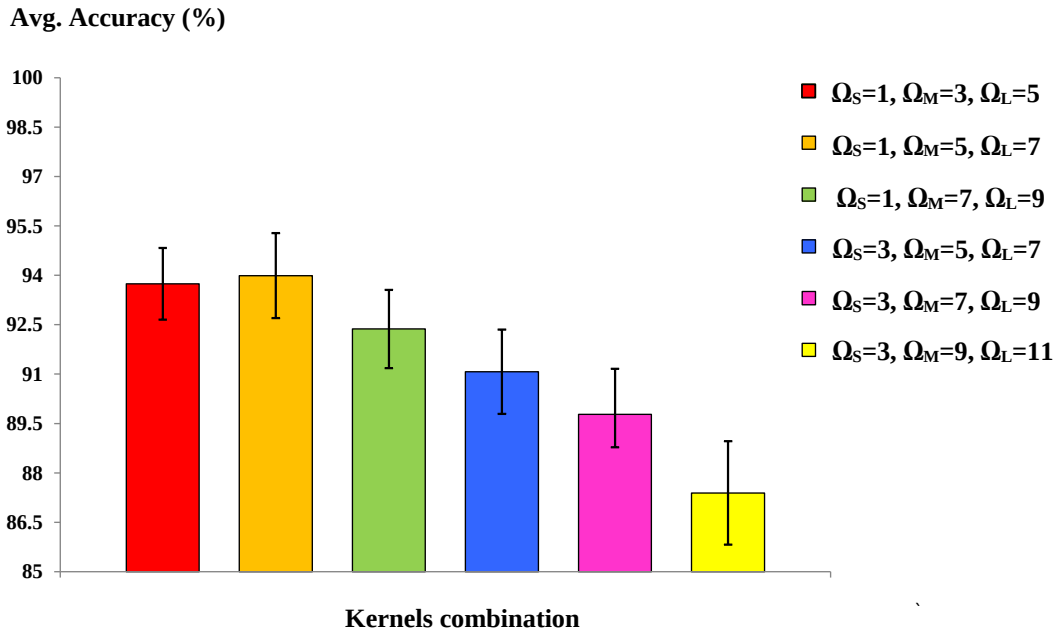

Figure 11: Comparison bar chart of average accuracy with SE (in %) for different combinations of convolutional kernel sizes in multi-scale convolution block (MSCB).

Table 4: Influence of different intrinsic feature extraction techniques on the average classification accuracy of the proposed MS-CNN model.

Average Accuracy with SE (%)			
No FE	**DE**	**NPS**	**All**
77.67 ±1.89	83.19 ±1.67	86.88 ±1.42	88.65±1.24

than the best result. Hence, the chosen combination of kernel sizes in MSCB optimizes the performance of the MS-CNN model in-terms of both classification accuracy and speed.

6.3 Influence of feature extraction : In this study, the influence of different feature extraction (FE) techniques on classification accuracy has been explored as shown in Table 4. At first, different feature extraction methods that include DE and NPS have been considered individually and the corresponding accuracy of the classifier has been determined. Finally, both the future extraction methods have been employed to obtain the final accuracy of the model. Note, DA methods have not been considered during this study. From the comparison in Fig. 12-(a), it is clear that feature integration significantly improves the accuracy of the model when accuracy increases 10.98% compared to the situation when the proposed model

Table 5: Influence of data augmentation methods on the average classification accuracy of the proposed MS-CNN model.

Average Accuracy with SE (%)					
No DA	**GN**	**S & R**	**WS**	**WW**	**All**
77.67 ±1.89	78.96 ±1.96	81.56 ±1.65	78.81±1.84	77.92±1.55	83.68±1.34

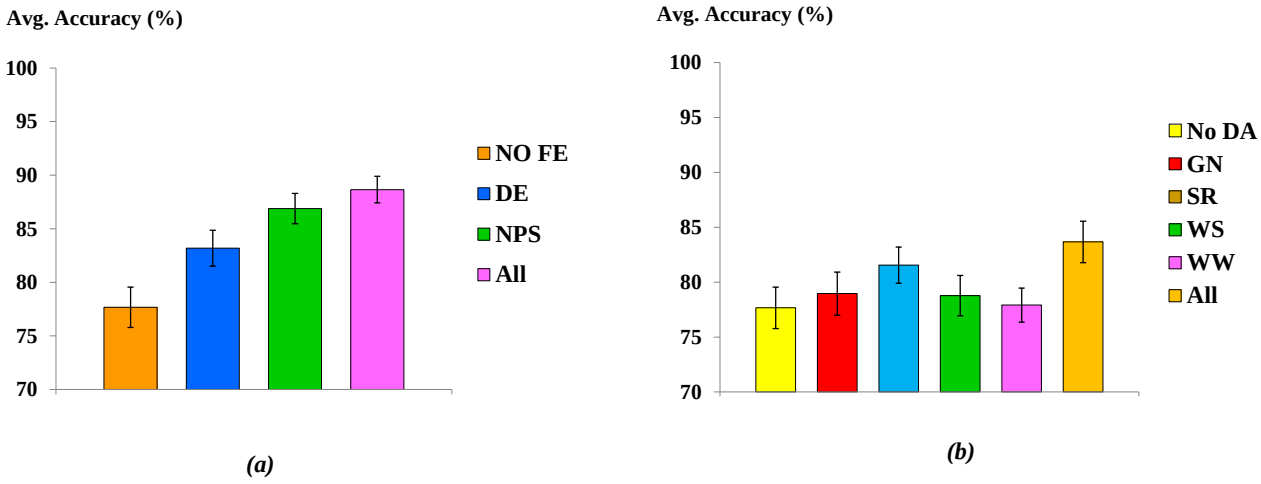

Figure 12: Comparison bar chart of average accuracy with SE (in %) for the influence of different (a) feature extraction techniques; (b) data augmentation methods in the proposed MI-BCI classification framework.

does not utilize any FE techniques. It is noteworthy to mention, the influence of NPS on the performance of the model is significant with 9.21% accuracy gain. From the analysis, it can be inferred that both DE and NPS FEs play an important role for improving overall performance of the MS-CNN model.

6.4 Influence of data augumentation methods: In the section, the influence of different data augmentation (DA) methods including Gaussian noise (GN), segmentation and recombination (S & R), window sliding (WS), and window wrapping (WW) have been evaluated on the performance of the classifier. Note, FE techniques have not been employed during the comparison. As shown in Table 5, the proposed model has reached the accuracy value of 77.67% without any DA. However, different DA methods improve the accuracy individually, in particular, there is a 3.89% accuracy gain by employing S & R. The combined effect of all DE methods demonstrated an overall 6.01% accuracy improvement indicating the importance of

Table 6: Comparison of the κ values for different subjects with existing state-of-the-art ML models with bold indicates the best result from the corresponding model.

Method	Subject									
	B01	**B02**	**B03**	**B04**	**B05**	**B06**	**B07**	**B08**	**B09**	**Avg**
CSP+EMD-SVM[66]	0.44	0.35	0.32	0.60	0.33	0.32	0.51	0.61	0.37	0.42
CSP-PSO based LSTSVM [63]	0.31	0.17	0.19	0.88	0.47	0.58	0.63	0.71	0.54	0.50
HT-SVM, LDA [65]	0.61	0.31	0.32	0.99	0.78	0.72	0.63	0.78	0.74	0.65
FBCSP-SVM[64]	0.48	0.29	0.25	0.97	0.98	0.70	0.67	0.84	0.79	0.66
WPD+SE-Isomap K-NN[16]	0.69	0.33	0.26	0.92	0.78	0.96	0.64	0.73	0.94	0.70
Proposed MS-CNN	0.92	0.867	0.89	0.95	0.94	0.91	0.94	0.92	0.95	0.92

proposed DA methods for achieving better performance and robustness of the current framework.

6.5 Comparison with different state-of-the-art ML models : In order to evaluate and compare with the performance of different ML classification models, average Cohen's kappa-coefficient (κ) has been utilized to measure the accuracy of the corresponding classifier. In Table 6, κ values obtained from the MS-CNN model have been compared with some of state-of-the-art machine learning models for BCI Competition IV 2b datasets. These ML models have utilized different feature extraction methodologies including CSP [63], filter bank CSP (FBCSP) [64], Hilbert transform (HT) [65], wavelet packet decomposition (WPD) [16], and empirical mode decomposition (EMD) algorithm considering different classification methods such as SVM [64, 66], least squares twin SVM (LSTSVM) [63], LDA [65], and K-NN [16]. From the overall comparison, it can be seen that the proposed MS-CNN model outshines other ML models significantly in terms of κ values for all nine subjects, as shown in Fig. 13. Comparing average κ, MS-CNN has achieved the highest κ value of 0.92 which is 22.2% and 26.01% improvement over the state-of-the-art ML methods in [16] and [64], respectively.

*Ref. [25] do not state accuracy values for each subject.

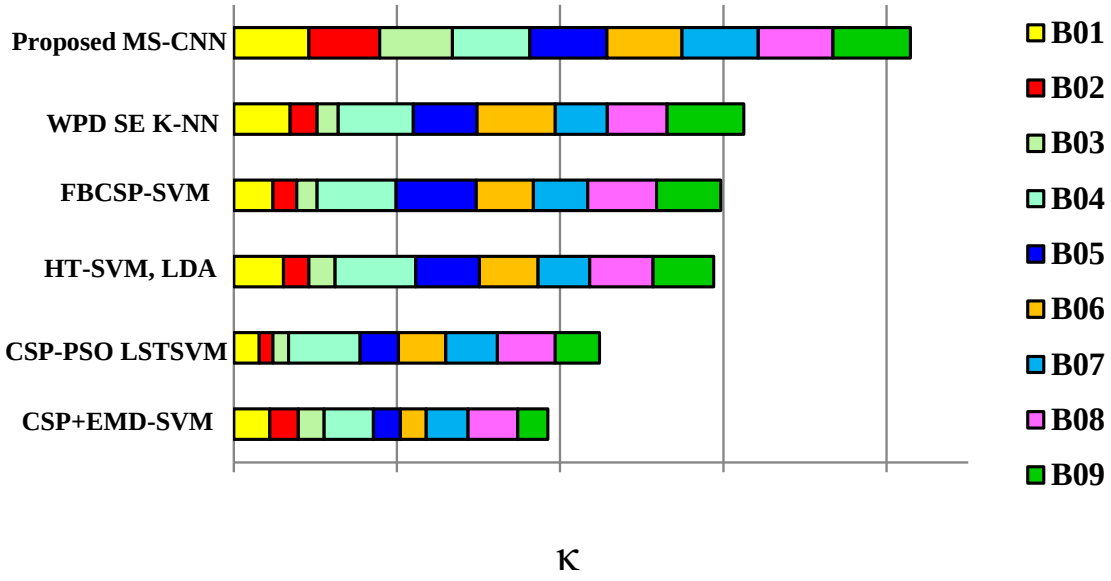

Figure 13: Comparison of κ values for each subject between the proposed model (MS-CNN) and other state-of-the-art ML models considering diffrent feature extraction methods and classification algorithms.

Table 7: Comparison of accuracy (in %) of different subjects with existing state-of-the-art DL models where bold indicates the best result from the corresponding model.

DL Model	Subjects									
	B01	**B02**	**B03**	**B04**	**B05**	**B06**	**B07**	**B08**	**B09**	**Avg.**
SCCNN* [25]	-	-	-	-	-	-	-	-	-	64.00
DTCNN[29]	72.6	60.3	66.9	91.2	80.6	70.6	73.2	77.7	71.2	73.77
CNN+SAE[14]	76.0	65.8	75.3	95.3	83.0	79.5	74.5	75.3	73.3	77.6
1DMSCNN[30]	80.56	65.44	65.97	99.32	89.19	86.1	81.25	88.82	86.81	82.61
FDBN[27]	81.0	65.0	66.0	98.0	93.0	88.0	82.0	94.0	91.0	84.0
HS-CNN[32]	80.5	70.6	85.6	94.6	98.3	86.6	89.6	95.6	87.4	87.6
Proposed MS-CNN	**93.4**	**88.7**	**89.1**	**95.3**	**95.1**	**93.8**	**94.7**	**96.8**	**96.7**	**93.74**

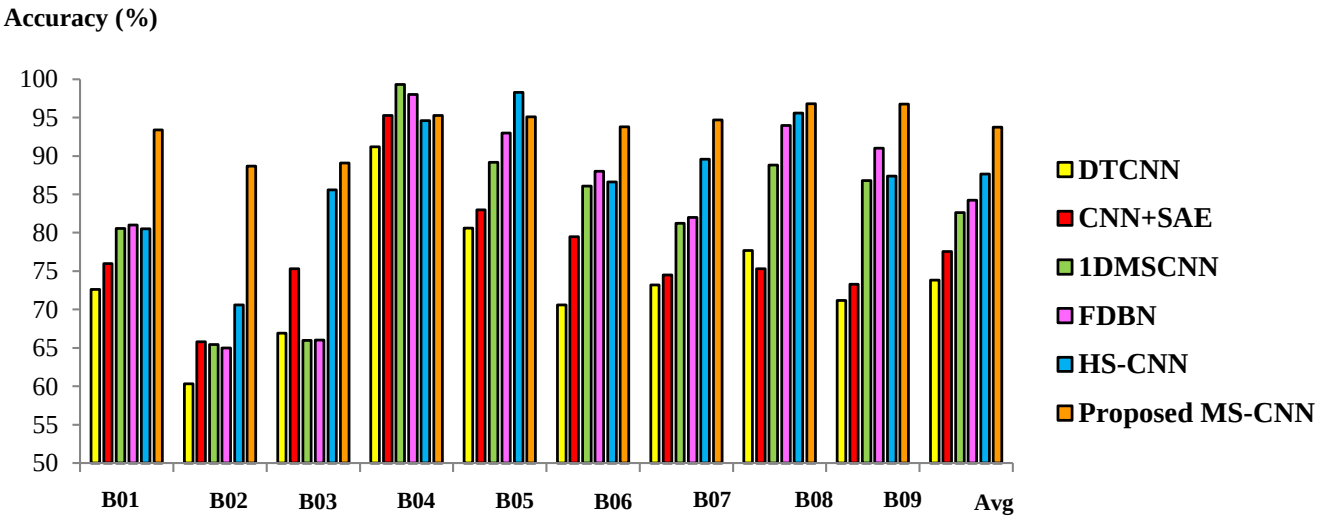

Figure 14: Comparison bar chart of the subject and average accuracy (in %) between proposed model (MS-CNN) and other state-of-the-art DL models for all different subjects.

6.6 Comparison with different state-of-the-art DL models : In this section, the accuracy of several state-of-the-art advanced DL models such as separated channel convolutional neural network (SCCNN)[25], deep transfer CNN (DTCNN) [29], CNN and stacked autoencoders (CNN+SAE) [14], 1-D multi-scale CNN (1DMSCNN) [30], frequential deep belief network (FDBN) [27], and hybrid-scale CNN (HS-CNN) [32] have been compared with the proposed model as detailed in Table 7. It can be seen that the proposed MS-CNN model attains the highest average classification accuracy of 93.74% among other DL models. It is noteworthy to mention that the proposed model improves the average classification accuracy of 11.13%, 9.74%, and 6.14% over the recent and more advanced DL models 1DMSCNN, FDBN and HS-CNN, respectively, as shown in Fig. 14. More specifically, MS-CNN demonstrated significant classification accuracy improvement in subject B01 (up to 12.9% increase), B02 (up to 18.1% increase), B06 (up to 7.2% increase), B09 (up to 9.3% increase) which indicates the efficiency and robustness of the proposed model. From the aforementioned comparison of classification accuracy and κ value, it can be inferred that the proposed MS-CNN model demonstrates better accuracy than the state-of-the-art different ML and advanced DL algorithms for all the subjects with the lowest SE. The result indicates the capability of subject-independent representation of EEG data and better generalization of the proposed classifier.

7. Discussion :

The current study demonstrates that MS-CNN with DA methods and feature integration techniques significantly improves the accuracy of two class MI-based BCI applications emphasizing the prospect of the current framework in adopting the distinguishable feature of MI-EEG signals. Additionally, the current model reduces the computational burden in MSCB and thus, increase the speed of the classifier. However, the present work focuses on MI-BCI classification tasks for the subject-dependent scenario, where the model has been trained and evaluated on the same subject. The future direction of the current work can be geared toward realizing subject-independent classification [67] where the evaluation phase is independent of the particular subject training class. Additionally, where high-performance person-independent classification is compulsory for the wide application of BCI Systems in the real-world, one possible solution to achieving the goal is to build a personalized model with transfer learning. An efficient transfer model can adopt a transductive parameter to construct an individual classifier which can be further extended to an adaptive-based transfer learning classifier [68]. Another direction could be the implementation of unsupervised or semi-supervised learning [69] to circumvent expensive and time-consuming manual labeling in unsupervised learning to perform classification tasks in abundant class labels for a wide range of MI-BCI scenarios. Moreover, in future work, classification accuracy can be further improved by integrating long short-term memory (LSTM) recurrent neural network (RNN) architecture [70] or self-attention based transformer [71] for extracting semantic temporal-spatial feature of EEG signal and expend the proposed framework for classifying multi-class MI for different BCI applications. Here, some important future research directions, in particular, geared toward the applications of BCI in the healthcare community have been acknowledged. Firstly, the current framework can be utilized in medical and health care, where the deep learning-based BCI systems predominantly work on the detection and diagnosis of mental diseases such as sleeping disorders, Alzheimer's Disease, epileptic seizure, and other disorders. The MS-CNN model can be widely adopted for its feature engineering and real-time classification for spontaneous EEG stream-based neurodegenerative diseases such as Parkinson's disease [72]. Moreover, the current model can be suitable for classifying AD based on spontaneous EEG [73] and diagnosis of an epileptic

seizure. In such scenarios, a hybrid model containing recurrent neural network (RNN) architecture attached to the MS-CNN model considering tempo-spatial feature extraction can be utilized in seizure diagnosis [74, 75]. Additionally, different mental diseases such as depression [76], Interictal Epileptic Discharge (IED) [77], schizophrenia [78], Creutzfeldt-Jakob disease (CJD) [79], and Mild Cognitive Impairment (MCI) [80] can be detected employing the current BCI deep learning model. Furthermore, the current framework can be extended as a more reliable and robust MI-based real-time brain signal based communications applications such as robotic control [5, 6, 7], P300 speller [81], rehabilitation of neuromotor disorders [4], text entry speech communication [8, 9], cognitive load measurement [82], gaming [2, 3] etc. The current model can be extended to various material modeling [83, 84, 85, 86, 87, 88, 89, 90]

8. Conclusion :

Summarizing, in this study, a multi-scale convolutional neural network has been designed for EEG-based MI classification. The multi-scale convolution block consisting of different convolutional kernel sizes in the proposed model can extract semantic features in multiple scales for different frequency bands δ, θ, α, and β from original EEG data for the classification purpose. Several intrinsic and user-specific features have been extracted from the original EEG data and integrated into the proposed algorithm to improve the accuracy and performance of the model. Furthermore, various data augmentation methods have been utilized to further improve the accuracy and robustness of the proposed classifier by increasing training EEG data. In order to validate the effectiveness of the framework, the proposed model has been applied to the BCI competition IV-2b dataset. Compared with other existing state-of-the-art algorithms, the classification accuracy of the current algorithm has been significantly improved. The results show that the proposed algorithm can attain high classification accuracy with the characteristic of similar performance among the different subjects. With average accuracy of 93.74%, the current framework demonstrates excellent classification performance and generalization. It improves the average classification accuracy of 11.13%, 9.74%, and 6.14% over the recent and more advanced DL models 1DMSCNN, FDBN and HS-CNN (with up to 18.1% increase of accuracy in the subject-specific case), respectively. The proposed model can extract more effective features from EEG signals and can be used to design the efficient and accurate real-time

MI-based BCI framework.

References

[1] Liu Z, Shore J, Wang M, Yuan F, Buss A, Zhao X (2021). A systematic review on hybrid EEG/fNIRS in brain-computer interface. Biomedical Signal Processing and Control, 68: 102595.

[2] Pan H, Mi W, Lei X, Deng J (2020). A closed-loop brain–machine interface framework design for motor rehabilitation. Biomedical Signal Processing and Control, 58: 101877.

[3] Sharma R, Kim M, Gupta A (2022). Motor imagery classification in brain-machine interface with machine learning algorithms: Classical approach to multi-layer perceptron model. Biomedical Signal Processing and Control, 71: 103101.

[4] Zhang Z, Sun J, Chen T (2022). A new dynamically convergent differential neural network for brain signal recognition. Biomedical Signal Processing and Control, 71: 103130.

[5] Wang H, Dong X, Chen Z, Shi BE (2015) Hybrid gaze/EEG brain computer interface for robot arm control on a pick and place task. 37th Annual International Conference of the IEEE Engineering in Medicine and Biology Society (EMBC) 1476–1479.

[6] Liao LD, Chen CY, Wang IJ, Chen S.F., Li SY, Chen BW, Chang JY, Lin CT (2012) Gaming control using a wearable and wireless EEG-based brain-computer interface device with novel dry foam-based sensors. Journal of Neuroengineering and Rehabilitation 9:5.

[7] LaFleur K, Cassady K, Doud A, Shades K, Rogin E, He B (2013) Quadcopter control in three-dimensional space using a noninvasive motor imagery-based brain–computer interface. Journal of Neural Engineering 10 (4):046003.

[8] Hossain MS, Amin SU, Alsulaiman M, Muhammad G (2019) Applying deep learning for epilepsy seizure detection and brain mapping visualization. ACM Trans Multimedia Comput Commun 1–17.

[9] Makin JG, Moses DA, Chang EF (2020) Machine translation of cortical activity to text with an encoder–decoder framework. Nature Neuroscience 23(4): 575-582.

[10] Xing J, Qiu S, Ma X, Wu C, Li J, Wang S, He H.(2020) A CNN-based comparing network for the detection of steady-state visual evoked potential responses. Neurocomputing 403:452-61.

[11] Pfurtscheller G, Brunner C, Schlogl A, Lopes da Silva FH (2006) Mu rhythm (de)synchronization and EEG single-trial classification of different motor imagery tasks. Neuroimage 31:153-9.

[12] Yu T, Xiao J, Wang F, Zhang R, Gu Z, Cichocki A, Li Y (2015). Enhanced motor imagery training using a hybrid BCI with feedback. IEEE Transactions on Biomedical Engineering 62 (7):1706–1717.

[13] Gandhi T, Panigrahi BK, Anand S (2011) A comparative study of wavelet families for EEG signal classification. Neurocomputing 74:3051–7.

[14] Tabar YR, Halici U (2017) A novel deep learning approach for classification of EEG motor imagery signals. J Neural Eng 14:016003.

[15] Luo J, Feng Z, Zhang J, Lu N (2016) Dynamic frequency feature selection based approach for classification of motor imageries. Comput Biol Med 75:45–53.

[16] Li M, Zhu W, Liu H, Yang J (2017) Adaptive Feature Extraction of Motor Imagery EEG with Optimal Wavelet Packets and SE-Isomap. Applied Sciences 7:390.

[17] Saa JFD, Çetin M (2012) A latent discriminative model-based approach for classification of imaginary motor tasks from EEG data. Journal of neural engineering 9:026020.

[18] Ang KK, Chin ZY, Zhang H, Guan C (2008) Filter Bank Common Spatial Pattern (FBCSP) in Brain-Computer Interface. 2008 IEEE International Joint Conference on Neural Networks 2390–7.

[19] Huang C, Tian G, Lan Y, Hao Y, Cheng Y, Peng Y, Che W (2019) A new Pulse Coupled Neural Network (PCNN) for Brain Medical Image Fusion empowered by Shuffled Frog Leaping. Frontiers in Neuroscience 13:210.

[20] Sturm I, Lapuschkin S, Samek W, Müller KR (2016) Interpretable deep neural networks for single-trial EEG classification. Journal of neuroscience methods 274:141–145.

[21] Schirrmeister RT, Springenberg JT, Fiederer LDJ, Glasstetter M, Eggensperger K, Tangermann M, Hutter F, Burgard W, Ball T (2017) Deep learning with convolutional neural networks for EEG decoding and visualization. Hum Brain Mapp 38:5391–5420.

[22] Chu Y, Zhao X, Zou Y, Xu W, Han J, Zhao Y (2018) A decoding scheme for incomplete motor imagery EEG with deep belief network. Frontiers in Neuroscience 12:680.

[23] Dose H, Møller JS, Iversen HK, Puthusserypady S (2018) An end-to-end deep learning approach to MI-EEG signal classification for BCIs. Expert Systems with Applications 114:532–542.

[24] Sun Y, Lo FPW, Lo B (2019) EEG-based user identification system using 1D–convolutional long short-term memory neural networks. Expert Systems with Applications 125:259–267.

[25] Zhu X, Li P, Li C, Yao D, Zhang R, Xu P (2019) Separated channel convolutional neural network to realize the training free motor imagery BCI systems. Biomed Signal Process Control 49:396–403.

[26] Xu B, Zhang L, Song A, Wu C, Li W, Zhang D, Xu G, Li H, Zeng H (2018) Wavelet trans- form time-frequency image and convolutional network-based motor imagery EEG classification. IEEE Access 7:6084–6093.

[27] Lu N, Li T, Ren X, Miao H (2017) A Deep Learning Scheme for Motor Imagery Classification based on Restricted Boltzmann Machines. IEEE Transactions on Neural Systems and Rehabilitation Engineering 25:566–76.

[28] Lawhern VJ, Solon AJ, Waytowich NR, Gordon SM, Hung CP, Lance BJ (2016) EEGNet: A Compact Convolutional Network for EEG-based Brain-Computer Interfaces. Journal of Neural Engineering 15:5.

[29] Xu G, Shen X, Chen S, Zong Y, Zhang C, Yue H, Liu M, Chen F, Che W (2019) A deep transfer convolutional neural network framework for EEG signal classification. IEEE Access 7:112767-112776.

[30] Tang X, Li W, Li X, Ma W, Dang X (2020) Motor imagery EEG recognition based

on conditional optimization empirical mode decomposition and multi-scale convolutional neural network. Expert Sys with Appl 149:113285.

[31] Nour M, Öztürk Ş, Polat K (2021) A novel classification framework using multiple bandwidth method with optimized CNN for brain–computer interfaces with EEG-fNIRS signals. Neural Comput Applic https://doi.org/10.1007/s00521-021-06202-4.

[32] Dai G, Zhou J, Huang J, Wang N (2020) HS-CNN: a CNN with hybrid convolution scale for EEG motor imagery classification. Journal of neural engineering 17(1):016025.

[33] Leeb R, Brunner C, MÃijller-PutzR G [Online]. Available: http://www.bbci.de/competition/iv/, Accessed on: March. 6, 2021.

[34] Klem GH, Lüders HO, Jasper HH and Elger C (1999) The ten-twenty electrode system of the International Federation. The International Federation of Clinical Neurophysiology Electroencephalogr Clin Neurophysiol Suppl 52:3–6.

[35] Tangermann M, Müller KR, Aertsen A, Birbaumer N, Braun C, Brunner C, Leeb R, Mehring C, Miller KJ, Mueller-Putz G (2012) Review of the BCI competition IV. Front Neurosci 6:55.

[36] Leeb R, Brunner C, Müller-Putz G, Schlögl A, Pfurtscheller G (2008) BCI Competition 2008–Graz data set B. Graz Univ Technol Austria 1–6.

[37] Dagdevir E, Tokmakci M (2021) Determination of Effective Signal Processing Stages for Brain Computer Interface on BCI Competition IV Data Set 2b: A Review Study. IETE Journal of Research 1-12.

[38] LeCun Y, Bengio Y and Hinton G (2015) Deep learning. Nature 521:436–44.

[39] Roy A.M. and Bhaduri J, (2021) A Deep Learning Enabled Multi-Class Plant Disease Detection Model Based on Computer Vision. AI 2(3): 413-428.

[40] Roy A.M., Bose R. and Bhaduri, J. (2021) A fast accurate fine-grain object detection model based on YOLOv4 deep neural network. arXiv preprint arXiv:2111.00298.

[41] Zhang X, Yao L, Sheng Z, Kanhere SS, Gu T, Zhang D (2018) Converting your thoughts to texts: Enabling brain typing via deep feature learning of EEG signals. In 2018 IEEE International Conference on Pervasive Computing and Communications (PerCom) 1–10.

[42] Donoghue T, Haller M, Peterson EJ, Varma P, Sebastian P, Gao R, Noto T, Lara AH, Wallis JD, Knight RT, Shestyuk A (2020) Parameterizing neural power spectra into periodic and aperiodic components. Nature neuroscience 23(12):1655-1665.

[43] Vuckovic A, Sepulveda F (2008) Delta band contribution in cue based single trial classification of real and imaginary wrist movements. Medical biological engineering computing, 46(6): 529-539.

[44] Reza A, Borhani S, Sellers EW, Jiang Y, Zhao X (2019) A comprehensive review of EEG-based brain–computer interface paradigms. Journal of neural engineering 16 (2019): 011001.

[45] Malan NS, Sharma S (2019) Feature selection using regularized neighbourhood component analysis to enhance the classification performance of motor imagery signals. Comput Biol Med 107:118–126.

[46] Shahid S, Sinha RK, Prasad G (2010) Mu and beta rhythm modulations in motor imagery related post-stroke EEG: a study under BCI framework for post-stroke rehabilitation. BMC Neurosci 11:127.

[47] Djemal R, Bazyed AG, Belwafi K, Gannouni S, Kaaniche W (2016) Three-Class EEG-Based Motor Imagery Classification Using Phase-Space Reconstruction Technique. Brain Sci 6(3):36.

[48] Liu YH, Lin LF, Chou CW, Chang Y, Hsiao YT, Hsu WC (2019) Analysis of Electroencephalography Event-Related Desynchronisation and Synchronisation Induced by Lower-Limb Stepping Motor Imagery. J Med Biol Eng 39:54–69.

[49] Weber E, Doppelmayr M (2016) Kinesthetic motor imagery training modulates frontal midline theta during imagination of a dart throw. International Journal of Psychophysiology 110:137–45.

[50] Szegedy C, Ioffe S, Vanhoucke V, Alemi AA (2017) Inception-v4, inception-resnet and the impact of residual connections on learning. Thirty-First AAAI Conference on Artificial Intelligence 4278–4284.

[51] Szegedy C, Liu W, Jia Y, Sermanet P, Reed S, Anguelov D, Erhan D, Vanhoucke V, Rabinovich A (2015) Going deeper with convolutions. In Proceedings of the IEEE conference on computer vision and pattern recognition 1–9.

[52] Sreeja SR, Rabha J, Nagarjuna KY, Samanta D, Mitra P, Sarma M (2017) Motor imagery EEG signal processing and classification using machine learning approach. In 2017 International Conference on New Trends in Computing Sciences (ICTCS) 61-66.

[53] Wang F, Zhong SH, Peng J, Jiang J, Liu Y (2018) Data augmentation for eeg-based emotion recognition with deep convolutional neural networks. In International Conference on Multimedia Modeling 82-93.

[54] Fawzi A, Samulowitz H, Turaga D, Frossard P (2016) Adaptive data augmentation for image classification. IEEE International Conference on Image Processing 3688–3692.

[55] Lotte F (2015) Signal Processing Approaches to Minimize or Suppress Calibration Time in Oscillatory Activity-Based Brain Computer Interfaces. Proceedings of the IEEE 103(6):871–90.

[56] Guennec AL, Malinowski S, Tavenard R (2016) Data Augmentation for Time Series Classification using Convolutional Neural Networks. ECML/PKDD Workshop on Advanced Analytics and Learning on Temporal Data, Sep 2016, Riva Del Garda, Italy.

[57] Iwana BK, Uchida S (2021, January) Time series data augmentation for neural networks by time warping with a discriminative teacher. In 2020 25th International Conference on Pattern Recognition (ICPR) 3558-3565.

[58] MNE v0.23 (2021) https://mne.tools/

[59] PyEEG (2021) https:// Pyeeg.sourceforge.net

[60] NeuroDSP (2021) neurodsp-tools.github.io (https://neurodsp-tools.github.io/neurodsp)

[61] FOOOF: foof-tools.github.io/foof/(https://fooof-tools.github.io/fooof/)

[62] Dornhege G, Millán JDR, Hinterberger T, McFarland D, Müller KR (2007) Toward brain-computer interfacing. Cambridge MA: MIT press.

[63] Li D, Zhang H, Khan MS, Mi F (2018) A self-adaptive frequency selection common spatial pattern and least squares twin support vector machine for motor imagery electroencephalography recognition. Biomed Signal Process Control 41:222–232.

[64] Luo J, Wang J, Xu R, and Xu K (2019) Class discrepancy guided sub-band filter-based common spatial pattern for motor imagery classification. J Neurosci Methods 323:98–107.

[65] Bagh N, Reddy MR (2020) Hilbert transform-based event related patterns for motor imagery brain computer interface. Biomed Signal Process Control 62:102020.

[66] Álvarez-Meza AM, Velásquez-Martínez LF, Castellanos-Dominguez G (2015) Time-series discrimination using feature relevance analysis in motor imagery classification. Neurocomputing 151:122–129.

[67] Kwon, O.-Y., Lee, M.-H., Guan, C., and Lee, S.-W. (2019). Subject-independent brain computer interfaces based on deep convolutional neural networks. IEEE transactions on neural networks and learning systems, 31(10):3839-3852.

[68] Zhang, K., Robinson, N., Lee, S.-W., and Guan, C. (2021). Adaptive transfer learning for EEG motor imagery classification with deep convolutional neural network. Neural Networks,136:1-10.

[69] [85] Xiaowei Jia, Kang Li, Xiaoyi Li, and Aidong Zhang. 2014. A novel semi-supervised deep learning framework for active state recognition on eeg signals. In Bioinformatics and Bioengineering (BIBE), 2014 IEEE International Conference on. IEEE, 30–37.

[70] Zhang, R., Zong, Q., Dou, L., Zhao, X., Tang, Y., and Li, Z. (2021). Hybrid deep neural network using transfer learning for EEG motor imagery decoding. Biomedical Signal Processing and Control, 63:102144.

[71] Vaswani, A., Shazeer, N., Parmar, N., Uszkoreit, J., Jones, L., Gomez, A.N., Kaiser, L. and Polosukhin, I., 2017. Attention is all you need. In Advances in neural information processing systems (pp. 5998-6008).

[72] Giulio Ruffini, David Ibanez, Marta Castellano, Stephen Dunne, and Aureli Soria-Frisch. 2016. EEG-driven RNN classification for prognosis of neurodegeneration in at-risk patients. In International Conference on Artificial Neural Networks. Springer, 306–313.

[73] Yilu Zhao and Lianghua He. 2014. Deep learning in the EEG diagnosis of Alzheimers disease. In Asian Conference on Computer Vision. Springer, 340–353.

[74] Adam Page, JT Turner, Tinoosh Mohsenin, and Tim Oates. 2014. Comparing Raw Data and Feature Extraction for Seizure Detection with Deep Learning Methods.. In FLAIRS Conference.

[75] JT Turner, Adam Page, Tinoosh Mohsenin, and Tim Oates. 2014. Deep belief networks used on high resolution multichannel electroencephalography data for seizure detection. In 2014 AAAI Spring Symposium Series.

[76] U Rajendra Acharya, Shu Lih Oh, Yuki Hagiwara, Jen Hong Tan, Hojjat Adeli, and D Puthankail Subha. 2018. Automated EEG-based screening of depression using deep convolutional neural network. Computer methods and programs in biomedicine 161 (2018), 103–113.

[77] Andreas Antoniades, Loukianos Spyrou, Clive Cheong Took, and Saeid Sanei. 2016. Deep learning for epileptic intracranial EEG data. In Machine Learning for Signal Processing (MLSP), 2016 IEEE 26th International Workshop on. IEEE, 1–6.

[78] Sergey M Plis, Devon R Hjelm, Ruslan Salakhutdinov, Elena A Allen, Henry J Bockholt, Je.rey D Long, Hans J Johnson, Jane S Paulsen, Jessica A Turner, and Vince D Calhoun. 2014. Deep learning for neuroimaging: a validation study. Frontiers in neuroscience 8 (2014), 229.

[79] Francesco Carlo Morabito, Maurizio Campolo, Nadia Mammone, Mario Versaci, Silvana Francesche.i, Fabrizio Tagliavini, Vito Sofia, Daniela Fatuzzo, Antonio Gambardella, Angelo Labate, and others. 2017. Deep learning representation from electroencephalography of Early-Stage Creutzfeldt-Jakob disease and features for di.erentiation from rapidly progressive dementia. International journal of neural systems 27, 02 (2017), 1650039.

[80] Heung-Il Suk, Chong-Yaw Wee, Seong-Whan Lee, and Dinggang Shen. 2016. State-space model with deep learning for functional dynamics estimation in resting-state fMRI. NeuroImage 129 (2016), 292–307.

[81] Koki Kawasaki, Tomohiro Yoshikawa, and Takeshi Furuhashi. 2015. Visualizing extracted feature by deep learning in P300 discrimination task. Computing and Pattern Recognition (SoCPaR), 2015 7th International Conference of. IEEE, 149–154.

[82] Pouya Bashivan, Mohammed Yeasin, and Gavin M Bidelman. 2015. Single trial prediction of normal and excessive cognitive load through EEG feature fusion. In Signal Processing in Medicine and Biology Symposium (SPMB), 2015 IEEE. IEEE, 1–5.

[83] Arunabha. M. Roy, JETP Letters 112, 173–179 (2020) DOI: https://doi.org/10.1134/S0021364020150023

[84] Arunabha. M. Roy, Applied Physics A, 126, 576 (2020) DOI: https://doi.org/10.1007/s00339-020-03742-9

[85] Arunabha. M. Roy, Materialia 15 (2021): 101000. DOI: https://doi.org/10.1016/j.mtla.2021.101000

[86] Arunabha. M. Roy, Journal of Applied Physics 129.2 (2021): 025103. DOI: https://doi.org/10.1063/5.0025867

[87] Arunabha. M. Roy, Phase field approach for multiphase phase transformations, twinning, and variant-variant transformations in martensite. PhD diss., Iowa State University, 2015. DOI: https://doi.org/10.31274/etd-180810-4187

[88] Arunabha. M. Roy, Physica B: Condensed Matter 615 (2021): 412986. DOI: https://doi.org/10.1016/j.physb.2021.412986

[89] Arunabha. M. Roy, EPL (Europhysics Letters), 133(5), 56001. DOI: https://doi.org/10.1209/0295-5075/133/56001

[90] Arunabha. M. Roy, JETP Letters 113.4 (2021): 265-272. DOI: https://doi.org/10.1134/S0021364021040032